# Electromagnetic characteristics of $A \leqslant 3$ physical and lattice nuclei

Johannes Kirscher,[1,2] Ehoud Pazy,[3] Jonathan Drachman,[1] and Nir Barnea[1]
[1]*The Racah Institute of Physics, The Hebrew University, 91904 Jerusalem, Israel*
[2]*Department of Physics, The City College of New York, New York, New York 10031, USA*
[3]*Department of Physics, NRCN, P.O.B. 9001, Beer Sheva 84190, Israel*
(Received 11 March 2017; revised manuscript received 1 June 2017; published 1 August 2017)

We analyze the quark-mass dependence of electromagnetic properties of two- and three-nucleon states. To that end, we apply the pionless effective field theory (EFT) to experimental data and numerical lattice calculations which simulate QCD at pion masses of 450 and 806 MeV. At the physical pion mass, we postdict the magnetic moment of helium-3, $\mu_{^3\mathrm{He}} = -2.13$ nNM (natural nuclear magneton), and the magnetic polarizability of deuterium, $\beta_{\mathrm{D}} = 7.3310^{-2}$ fm$^3$. Magnetic polarizabilities of helium-3, $\beta_{^3\mathrm{He}} = 9.710^{-4}$ fm$^3$, and the triton, $\beta_{^3\mathrm{H}} = 8.210^{-4}$ fm$^3$, are predictions. Postdictions of the effective theory for the magnetic moments are found consistent with QCD simulations at 806 MeV pion mass, while our EFT result $\beta_{\mathrm{D}} = 2.9210^{-2}$ fm$^3$ was not extracted from the lattice. The deuteron would thus be relatively pliable compared to a three-nucleon state for which we postdict $\beta_{^3\mathrm{H}} = 3.910^{-5}$ fm$^3$. At $m_\pi = 450$ MeV, the magnetic moment of the triton is predicted, $\mu_{^3\mathrm{He}} = -2.15(5)$ nNM, based on a conjecture of its binding energy, $B_{^3\mathrm{H}} \cong 30$ MeV. For all three pion masses, we compare the point-charge radii of the two- and three-nucleon bound states. The sensitivity of the electromagnetic properties to the Coulomb interaction between protons is studied in anticipation of lattice calculations with dynamical QED.

DOI: 10.1103/PhysRevC.96.024001

## I. OVERTURE

Knowledge regarding the orbital angular momenta and spin orientations of the nucleons, bound in the core of an atom, led to a quantitative understanding of the (hyper)fine structure of the electron shell, i.e., atomic spectra, and the dynamics of nuclei in external electromagnetic fields. The pioneering experiments on nuclear magnetic moments were based purely on their electromagnetic interaction, e.g., inferring the dependence of resonance frequencies of hydrogen molecules on an external magnetic field [1]. Such experiments helped thereby to parametrize nuclear properties in terms of the fundamental constants of quantum electrodynamics (QED). The lattice quantum chromodynamics (LQCD) calculations of the same observables, i.e., responses of nuclei to external fields, assume analogously the validity of QCD for nuclei and parametrize them in terms of the constants of the strong interaction. While both experiment and QCD, in principle, yield the desired property of every nucleus, clearly not all experiments nor all LQCD extractions are practical. The predictions which were initially made to fill in these gaps were based on pairing models for closed-shell nuclei [2] and required a determination of only the neutron and proton magnetic moments. Refinements [3] of this model gave insight to the structural details of few-nucleon wave functions, e.g., $D$-state admixtures [4]. The fundamental correlation between nuclear wave functions and electromagnetic responses is part of the description of nuclei in terms of effective field theories (EFTs). Matching these EFTs to LQCD data is believed to yield a predictive *theory*.

In this article, we apply a candidate for such a theory EFT($\not\pi$), as developed in Refs. [5–9], to analyze the structure of two and three-nucleon systems through their interaction with external electromagnetic probes. The availability of LQCD calculations at unphysically large quark/pion masses is combined with experimental data to assess the dependence of charge radii, magnetic moments, and polarizabilities on nucleon masses, deuteron-triton binding-energy splittings, and bound states in the two-nucleon singlet channels. Furthermore, we assess the expected gain in accuracy from dynamical QED, incorporated into the LQCD extractions of these observables.

## II. INTERACTION BETWEEN NUCLEONS AND THE ELECTROMAGNETIC FIELD

Based on the nonrelativistic character of nucleons as constituents of nuclear bound states, their interaction with external electromagnetic fields and charged nucleons can be described through a combination of EFT($\not\pi$) with nonrelativistic quantum electrodynamics (NRQED) [10]. The Lagrangian of this effective nuclear theory is expressed in terms of an isospin doublet field $N = \binom{p}{n}$, which comprises a two-component Pauli spinor for the proton ($p$) and the neutron ($n$), as the most general density conceivable under the constraints of gauge invariance, locality, hermiticity, parity conservation, time-reversal symmetry, and Galilean invariance. To leading order (LO) in the strong interaction and to order $1/m$ in the Foldy-Wouthuysen-Tani expansion of the Dirac theory, the effective theory, as relevant for the $A$-nucleon one-photon sector, reads [6]

$$\begin{aligned}\mathcal{L} = N^\dagger \Big\{ & i\partial_0 - e\hat{Q}A_0 + \frac{1}{2m}(\boldsymbol{\partial} - ie\hat{Q}\boldsymbol{A})^2 + \hat{g}_N \frac{e}{2m}\boldsymbol{\sigma}\cdot\boldsymbol{B} \Big\} N \\ & + \frac{c_T}{m\not\pi}(N^T P_i N)^2 + \frac{c_S}{m\not\pi}(N^T \bar{P}_3 N)^2 + \frac{d_3}{m\not\pi^4}(N^\dagger)^3(N)^3 \\ & + l_1 \frac{e}{m m_\pi}(N^T P_i N)^\dagger (N^T \bar{P}_3 N) B_i \\ & + l_2 \frac{e}{m m_\pi} i\epsilon_{ijk}(N^T P_i N)^\dagger (N^T P_j N) B_k . \end{aligned} \tag{1}$$

 

Where, here, and throughout this work, neutrons and protons are assumed to have the same (quark mass dependent) mass $m = m(m_\pi)$. $\boldsymbol{A},\boldsymbol{B}$ are the three-dimensional electromagnetic vector potential and magnetic fields, $\hat{Q} = \frac{1}{2}(1+\tau_3)$ is the charge operator, and $\hat{g}_N = g_{p/n}(1 \pm \tau_3)$ the single-particle magnetic moment. $P_i$ and $\bar{P}_3$ are projections onto two-nucleon spin triplet and singlet states, respectively.

Three bare low-energy constants (LECs) $c_S, c_T, d_3$ parametrize the strong interaction and need to be determined by a matching procedure as well as the four LECs, $\{g_p, g_n, l_1, l_2\}$, which couple the gauge field to the nucleon(s). Without its kinetic terms, the radiation field is static. In the Coulomb gauge, the equation of motion for $A_0$ is time independent and can be integrated to yield

$$A_0(\boldsymbol{r},t) = e \int \frac{N^\dagger(\boldsymbol{r}',t)N(\boldsymbol{r}',t) + \rho_{\text{ext}}(\boldsymbol{r}',t)}{|\boldsymbol{r}-\boldsymbol{r}'|} d\boldsymbol{r}', \quad (2)$$

where the total charge density in the numerator may contain dynamical and static ($\rho_{\text{ext}}$) parts. The former constitutes the Coulomb interaction if substituted in the second term of the Lagrangian. Through the static distribution $\rho_{\text{ext}}$ the single-nucleon current is coupled to an external charge. Matrix elements of this operator are usually parameterized by the point-charge radius (see below). The unnatural scaling of the interaction terms with respect to a peculiar low-energy scale $\aleph \sim 1/a_s$ ($a_s$ is the scattering length), and a breakdown scale of the order of the pion mass $m_\pi$ demands a nonperturbative treatment of the three strong LECs, while the four magnetic couplings are perturbative.[1] Of the latter, the two-body parameters $l_1, l_2$ are suppressed by $1/m_\pi$ relative to the one-body terms $g_{n/p}$. The range of applicability of this theory constrains the momenta of the interacting nucleons to values below $\sim m_\pi/2$. Within this range, the Coulomb interaction is nonperturbative for momenta $\lesssim e^2 m/4\pi$ [11] and requires an additional counterterm. For momenta of the order of $e^2 m/4\pi$ or larger, e.g., in the helion bound state [12,13], the interaction is perturbative. The Lagrangian, subject to these rules, defines EFT($\not\pi$) for the description of light nuclei in the presence of an external magnetic field and Coulomb-interacting protons. For practical few-nucleon calculations, we translate the Lagrangian and the power counting into a nuclear Hamiltonian $\hat{H}_{\text{nucl}}$ and an interaction Hamiltonian $\hat{H}_{\text{nucl-}B}$ between the nucleons and the magnetic background field:

$$\hat{H}_{\text{nucl}} = -\sum_i^A \frac{\nabla_i^2}{2m} + \sum_{i<j}^A \hat{V}_{2b}(ij) + \sum_{i<j<k}^A \sum_{\text{cyc}} \hat{V}_{3b}(ijk), \quad (3)$$

where $\hat{V}_{2b}$, $\hat{V}_{3b}$ are the two- and three-body potentials,

$$\hat{V}_{2b}(ij) = \left[c_S^\Lambda \frac{1}{4}(1 - \boldsymbol{\sigma}_i \cdot \boldsymbol{\sigma}_j) + c_T^\Lambda \frac{1}{4}(3 + \boldsymbol{\sigma}_i \cdot \boldsymbol{\sigma}_j)\right]\delta_\Lambda(\boldsymbol{r}_{ij}) + \left[c_{pp}^\Lambda \delta_\Lambda(\boldsymbol{r}_{ij}) + \frac{e^2}{r_{ij}}\right]\frac{1}{4}(1+\boldsymbol{\tau}_{i,z})(1+\boldsymbol{\tau}_{j,z}) \quad (4)$$

and

$$\hat{V}_{3b}(ijk) = d_3^\Lambda \delta_\Lambda(\boldsymbol{r}_{ij}, \boldsymbol{r}_{ik}). \quad (5)$$

[1]We assume $e|\boldsymbol{B}| \ll m m_\pi \sim 10^{17}\ \text{GeV}^2 \sim 10^{18}$ G.

We chose delta functions to be approximated by Gaussians with parameter $\Lambda$,

$$\delta_\Lambda(\boldsymbol{r}_{ij}) = e^{-\frac{\Lambda^2}{4}\boldsymbol{r}_{ij}^2}$$
$$\delta_\Lambda(\boldsymbol{r}_{ij}, \boldsymbol{r}_{ik}) = e^{-\frac{\Lambda^2}{4}(\boldsymbol{r}_{ij}^2 + \boldsymbol{r}_{ik}^2)}. \quad (6)$$

We vary $\Lambda$ for an estimate of the renormalization-group dependence of observables. For this estimate, no theoretical upper bound on $\Lambda$ exists. Due to the few-body methods, we set a practical limit of 15 fm$^{-1}$. If $\Lambda$ is chosen too small, important contributions to an $A$-body amplitude might be cut off. Based on the estimate that the lowest $A$-body pole corresponding to a binding energy $B_A$ demands intermediate two-nucleon momenta of about $\sqrt{2mB_A/A}$ [14], we used $\Lambda \gtrsim 2$ fm$^{-1}$ which exceeds this bound for all considered $A \leqslant 3$ observables and pion masses.

The interaction between the nucleons and the magnetic field is expressed through the magnetization density current

$$\hat{H}_{\text{nucl}-B} = (\boldsymbol{\mu}^{(1)} + \boldsymbol{\mu}^{(2)}) \cdot \boldsymbol{B}, \quad (7)$$

where

$$\boldsymbol{\mu}^{(1)} = \sum_{i=1}^A \mu_N \left(\frac{g_p + g_n}{2}\boldsymbol{\sigma}_i + \frac{g_p - g_n}{2}\boldsymbol{\sigma}_i \tau_{i,z}\right) \quad (8)$$

and

$$\boldsymbol{\mu}^{(2)} = \sum_{i<j}^A \mu_N \left[l_1^\Lambda (\boldsymbol{\sigma}_i - \boldsymbol{\sigma}_j)(\tau_{i,z} - \tau_{j,z}) + l_2^\Lambda (\boldsymbol{\sigma}_i + \boldsymbol{\sigma}_j)\right]\delta_\Lambda(\boldsymbol{r}_{ij}). \quad (9)$$

$\mu_N = |e|\hbar/2mc$ is the $m_\pi$ dependent, natural nuclear magneton (nNM). The process of eliminating the $\Lambda$ dependence for a set of observables by absorbing it into the LECs is indicated by the superscripts. Divergences from the above-mentioned nonlocal Coulomb repulsion are renormalized by $c_{pp}^\Lambda$. Like the nucleon mass and the proton charge, the gyromagnetic factors $g_p, g_n$ of the nucleons substitute bare LECs. Projection operators for the two- and three-nucleon channels are written explicitly with standard SU(2) (iso)spin matrices.

To solve the two- and three-body Schödinger equation with $\hat{H}_{\text{nucl}}$ in order to determine bound and scattering states whose properties are used to calibrate the LECs, and whose $\hat{H}_{\text{nucl-}B}$ matrix elements yield their leading electromagnetic characteristics, we employ two numerical techniques: the effective-interaction hyperspherical-harmonic (EIHH) method [15,16], and the refined resonating-group ($\mathbb{R}$GM) method [17]. Details of the numerical implementation of both methods can be found in Ref. [18] and references therein. Besides benchmarking the two numerical techniques, we compare their results with an analytic two-nucleon calculation in the so-called zero-range approximation which is identical to EFT($\not\pi$) for an infinite regulator $\Lambda$.

Having defined the formal structure and the algorithms used to solve the theory, we specify observables presumably within its range of applicability in order to, first, calibrate the LECs, and second, exploit their predictive power. As in Ref. [18], we investigate three different realizations of the standard model, and thereby the quark-mass dependence of light nuclei. First,

we determine the LECs for the natural ($m_\pi = 137$ MeV) case, by matching to experimental data. The strong interaction parameter $c_T$ is tuned to the deuteron binding energy, $c_S$ to the neutron-proton-singlet scattering length, and $d_3$ to the triton binding energy. The magnetic parameters are chosen to yield the magnetic moments of the triton ($l_1$) and the deuteron ($l_2$).

Second, we match to lattice QCD predictions for SU(3)-degenerate quarks with a mass corresponding to $m_\pi = 806$ MeV. At this $m_\pi$, all two-nucleon singlet states are bound. The LEC $c_S$ is thus adapted to reproduce the $np$ singlet binding energy. If the magnetic field is nonzero, the eigenstates are no longer states with well defined spin. As long as the fields support bound states in the singlet and triplet channels, the eigenstates will be superpositions of the two. This was realized in Ref. [19] where the operator basis for the extraction of the two-nucleon ground state included sink and source interpolating fields with different total spin. The diagonalization of the ensuing correlation matrix yielded eigenstates with energies split by $\Delta E_{^3S_1,\,^1S_0}$. This splitting can be related to the EFT $\ell_1$ LEC as follows. For $\boldsymbol{B} = 0$, the Hamiltonian sustains two $np$ $S$-wave bound states $|0\rangle, |1\rangle$ with total angular momentum $j = 0, 1$ and energies $B_{np}, B_D$. For $\boldsymbol{B} \neq 0$, the operator $\boldsymbol{\mu} \cdot \boldsymbol{B}$ couples the two channels for $m_j = 0$ and shifts the energy eigenvalues to

$$B_\pm = \frac{1}{2}\left(B_{\rm D} + B_{np} \pm \sqrt{(B_{\rm D} - B_{np})^2 + 4t_{01}^2 |\boldsymbol{B}|^2}\right) \times \overset{B_{\rm D}-B_{np} \ll |\boldsymbol{B}|}{\approx} \frac{(B_{\rm D} + B_{np})}{2} \pm t_{01}|\boldsymbol{B}|, \tag{10}$$

with $t_{01} = \langle 0|\boldsymbol{\mu} \cdot \hat{\boldsymbol{B}}|1\rangle$. Using Eq. (7), the energy split is thus parametrized with $l_1$:

$$\Delta E_{^3S_1,\,^1S_0} = \langle 0|\boldsymbol{\mu} \cdot \boldsymbol{B}|1\rangle = |\boldsymbol{B}|[(g_p - g_n)\langle \varphi^{(np)}|\varphi^{(D)}\rangle + 4l_1 \langle \varphi^{(np)}|\delta_\Lambda(r)|\varphi^{(D)}\rangle], \tag{11}$$

with $\varphi^{(np/D)}$ being the radial wave functions of the singlet/triplet states. The magnetic parameter $l_1$ can thereby alternatively be tuned to reproduce this energy split. All other LECs are fitted to the same observables as at physical pion mass.

For the intermediate pion mass $m_\pi = 450$ MeV, two-nucleon LQCD binding energies constrain $c_S, c_T$. Data input for the magnetic couplings, $\mu_{\rm D}$, $\mu_{^3{\rm H}}$, and $t_{01}$, is unavailable. Assuming a linear dependence of $l_{1,2}$ on $m_\pi$, we interpolate linearly between the fitted values at physical $m_\pi$ and 806 MeV pion mass. We interpolated separately for each cutoff value, and thereby translated an EFT uncertainty to $m_\pi = 450$ MeV. This assumption is based on the hypothesis of the pion-mass-independent existence of a shallow two-nucleon state. The magnetic moment of such a state is quite accurately reproduced in the shell-model approximation. The $l_{1,2}$ corrections will then be relatively small in units of natural nuclear magnetons.

A comment about the Coulomb interaction between protons is in order. While the proton-proton scattering length and the $^3$He binding energy are known experimentally, LQCD calculations which consider some version of QED for the electromagnetic interaction of the quarks are, as of now, unattainable. In order to estimate the effect of dynamical U(1) gauge fields, we proceed as follows. We assume that QCD corrections to the QED fine-structure constant $\alpha$ are insignificant for the accuracy of this work. What justifies the perturbative treatment of the Coulomb force for physical $^3$He holds also for the bound two and three-nucleon states containing two protons, i.e., the $pp$ singlet, and $^3$He with heavier pions. These systems should even be more amenable to a perturbative expansion because of the larger binding momenta associated with their binding energies (Table I). An ansatz for the effective interaction resultant from quark QED as a Coulomb exchange, whose iterations should be strongly suppressed in bound states, and a counterterm to renormalize low-energy amplitudes, seems appropriate. We expect this "model" to shift the di-proton binding energy by the amount an iterated Coulomb interaction with $\alpha = \alpha_{\rm physical}$ determines, plus a correction from $c_{pp}$ to eliminate cutoff dependence. We fixed $c_{pp}^\Lambda$ by enforcing the split $B(np) - B(pp) = 0.5$ MeV. As this differs from a splitting induced by Coulomb by $\ll 1$ MeV over the considered cutoff range (see discussion of Fig. 1), we cannot discriminate the ensuing $c_{pp}$ from other values which set the splitting at values which differ by $\sim$1 MeV. All choices for the splitting correspond to different effective QED models,

TABLE I. Experimental and LQCD data for binding energies (MeV), magnetic moments (nNM), the two-body transition matrix element $t_{01}$ (nNM), and scattering lengths (fm).

| Observable | Nature [20] $m_\pi = 137$ MeV | LQCD $m_\pi = 450$ MeV [21–23] | LQCD $m_\pi = 806$ MeV [19,24] |
|---|---|---|---|
| $m$ | 938.9 | 1226(12) | 1634(18) |
| $\mu_n$ | −1.913 | −1.908(38) | −1.981(19) |
| $\mu_p$ | 2.793 | 2.895(56) | 3.119(74) |
| $B_{np}$ | | 12.5(50) | 15.9(40) |
| $a_{np}^{\rm singlet}$ | −23.75 | | |
| $a_{pp}$ | −7.806 | | |
| $B_{\rm D}$ | 2.225 | 14.4(32) | 19.5(48) |
| $\mu_{\rm D}$ | 0.857 | | 1.22(10) |
| $t_{01}$ | | | 5.48(20) |
| $B_{^3{\rm H}}$ | 8.482 | | 53.9(107) |
| $\mu_{^3{\rm H}}$ | 2.979 | | 3.56(19) |
| $B_{^3{\rm He}}$ | 7.718 | | |
| $\mu_{^3{\rm He}}$ | −2.127 | | |

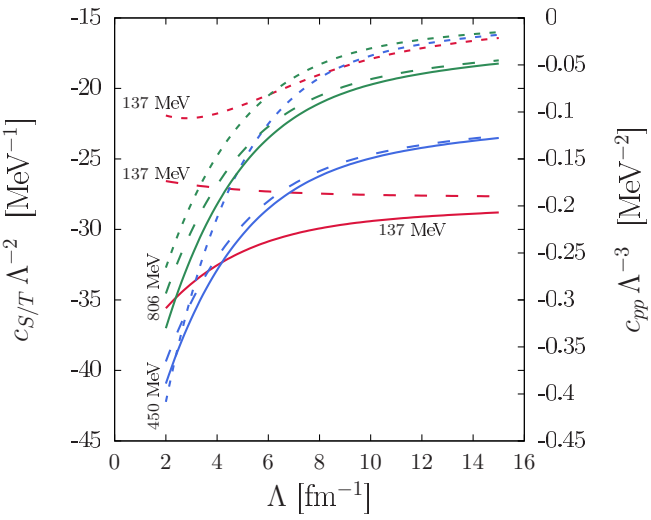


FIG. 1. Cutoff dependence of the LECs $c_S$ (solid line, left $y$ axis), $c_T$ (dashed line, left $y$ axis), and $c_{pp}$ (short-dashed line, right $y$ axis) for three pion masses, $m_\pi = 137$ MeV (red), $m_\pi = 450$ MeV (blue), and $m_\pi = 806$ MeV (green).

of which we assess two: $c_{pp}$ to yield the 0.5 MeV splitting and $c_{pp} = 0$ to yield an insignificantly $\Lambda$-dependent splitting $\lesssim$1 MeV.

## III. RESULTS

The EFT defined above is utilized to pre/postdict electromagnetic characteristics of the proton-proton, the singlet-neutron-proton, the deuteron, triton, and helium systems in the form of point-charge radii, magnetic moments, and magnetic polarizabilities. Numerical results are compiled in Table II as obtained for the three pion masses where enough data is available to renormalize the EFT. The uncertainties are to be viewed as lower bounds as they are inferred solely from the $\Lambda$ sensitivity. For the consistency analysis discussed in Sec. III A, we also considered the uncertainty in the input data but used the central LEC values for subsequent calculations.

### A. Low-energy constants and data consistency

The renormalization of the EFT demands regulator independence of a set of observables. With this set taken as specified in the previous section, we obtain a cutoff dependence of the LECs as shown in Fig. 1 for $c_S$,$c_T$,$c_{pp}$, and Fig. 2 for $l_1$,$l_2$. The numerical values of these LECs are presented in Appendix A. For a thorough discussion of the behavior of $c_S$,$c_T$, namely, the dominating $\Lambda^2$ dependence and the small Wigner-SU(4)-symmetry breaking component (overlapping solid and dashed lines in Fig. 1 for $\Lambda \to \infty$), we refer the reader to Ref. [18]. A different dependence of the small correction term $c_{pp}$ in the proton-proton channel is found here: an asymptotic behavior (short dashed lines, right $y$ axis in Fig. 1) for all three pion masses of $\lim_{\Lambda\to\infty} c_{pp} \propto \Lambda^3$. This unmasks the difference of the divergence structure of the Coulomb exchange as found in Ref. [11] relative to that of a two-nucleon loop. The latter is absorbed into $c_S$,$c_T$, while $c_{pp}$ is needed if the bubble is cut by a static Coulomb exchange.

A comment about previous calculations which demand $c_{pp}$ is in order. Here, we find $c_{pp}$ to adjust $c_S$ by less than 0.1% (compare scales in Fig. 1) over the considered cutoff range from 2 to 15 fm$^{-1}$. Despite the enhanced effect on observables,

TABLE II. EFT($\not\pi$) results ($\Lambda \to \infty$ extrapolations) for point-proton charge radii ($r_{\rm ch} \equiv \langle r_p^2\rangle^{1/2}$ fm), magnetic moments (nNM), and polarizabilities (fm$^3$). Preexisting experimental [20] or LQCD values [19] are written below EFT postdictions. Single entries represent true EFT predictions. Uncertainties result from $\Lambda$ variations.

| | | $m_\pi = 137$ MeV | $m_\pi = 450$ MeV | $m_\pi = 806$ MeV |
|---|---|---|---|---|
| $NN$ singlet | $r_{\rm ch}$ | | 0.588(260) | 0.458(240) |
| deuteron | $r_{\rm ch}$ | 1.55(24) | 0.550(250) | 0.416(250) |
| | | Expt. 1.97 | | |
| | $\beta_M$ | 0.0733(1) | | $2.92(1)10^{-2}$ |
| | | sum rule [25] 0.072 | | |
| | | AV18 [26] 0.0774 | | |
| | | EFT [27] 0.096 | | |
| triton | $r_{\rm ch}$ | 1.16(23) | 0.767(310) | 0.460(280) |
| | | Expt. [28] 1.55 | | |
| | | LO-EFT [29] 1.13(34) | | |
| | $\mu$ | 2.979 | 3.08(6) | 3.41(3) |
| | | Exp. 2.979 | | LQCD 3.56(18) |
| | $\beta_M$ | $8.2(1)10^{-4}$ | | $3.9(4)10^{-5}$ |
| | | | | LQCD $2.6(18)10^{-4}$ |
| helion | $r_{\rm ch}$ | 1.30(28) | 0.793(300) | 0.472(290) |
| | | Expt. 1.78 | | |
| | $\mu$ | $-2.13(1)$ | $-2.15(5)$ | $-2.17(6)$ |
| | | Expt. $-2.127$ | | LQCD $-2.29(12)$ |
| | $\beta_M$ | $9.7(1)10^{-4}$ | | $3.9(4)10^{-5}$ |
| | | | | LQCD $5.4(21)10^{-4}$ |

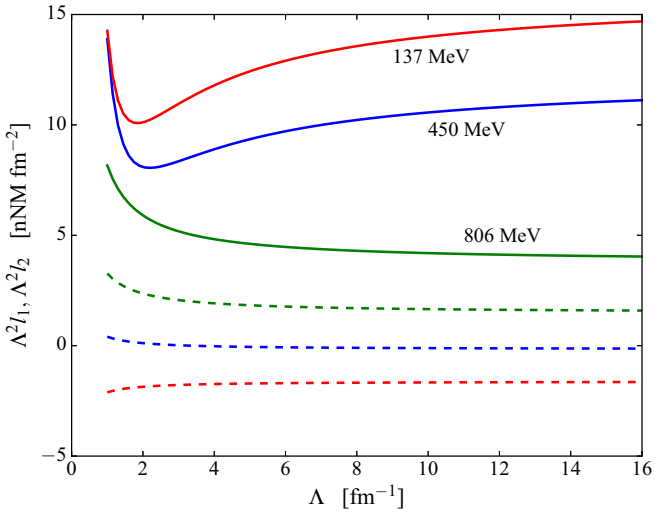


FIG. 2. Cutoff dependence of the LECs $l_1$ (solid line), and $l_2$ (dashed line) for three pion masses, $m_\pi = 137$ MeV (red), $m_\pi = 450$ MeV (blue), and $m_\pi = 806$ MeV (green). The values for $m_\pi = 137$ MeV, and $m_\pi = 806$ MeV are fitted to experimental and LQCD date respectively. The $m_\pi = 450$ MeV values are results of an interpolation.

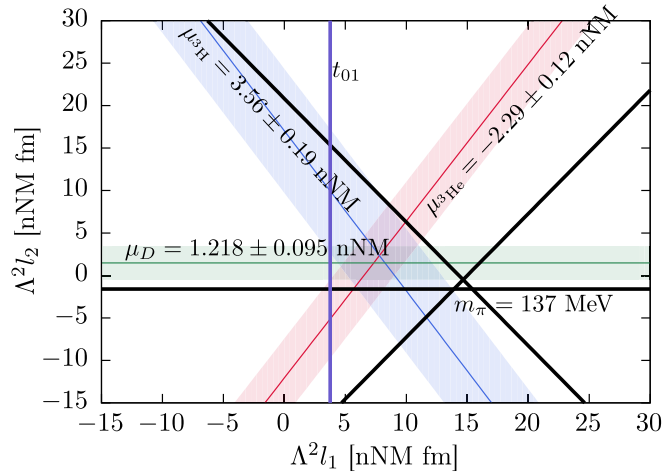


FIG. 3. Interdependence of two-body LECs consistent with the magnetic moments of the deuteron (green, horizontal), the triton (blue, negative slope), $^3$He (red, positive slope), and the magnetic-field contribution to the dinucleon energy splitting $\delta E_{^3S_1,\,^1S_0}$ (purple, vertical) at $m_\pi = 806$ MeV. The bandwidth resembles the total lattice uncertainty in the respective observable. The black lines marks the LEC values which yield the experimental deuteron, triton, and 3-helium magnetic moments at the physical pion mass.

setting $c_{pp} = 0$, as in Ref. [30], does not indicate a severe cutoff dependence, e.g., in predictions for the $^3$He binding energy or the proton-proton scattering length. This fallacy is a consequence of the specific regularization chosen here, and was avoided in, e.g., Ref. [31] with a different scheme, and in Ref. [12] with the same formalism as employed in this work. Within our scheme, we find the divergence only by splitting the LEC in the $pp$ channel as shown.

For the coupling of the photon to the two-nucleon vertex, i.e., $l_1$,$l_2$, we observe an asymptotic behavior of $\lim_{\Lambda\to\infty} l_i \propto \Lambda^{-2}$. This dependence can be derived analytically by understanding the limit $\Lambda \to \infty$ as the well-known zero-range approximation (see Appendix B). Another peculiarity at the largest pion mass is the sign difference of $l_2$ compared to the physical point. This is understood from the comparison of the deuteron's magnetic moment to those of its constituents. At leading order, $\mu_\mathrm{D} = \mu_p + \mu_n$, which is larger than the experimental value but smaller than the lattice measurement at $m_\pi = 806$ MeV. The next-to-leading-order (NLO) $l_2$ term thus either reduces or enlarges $\mu_\mathrm{D}$. To attest to the consistency of the theory with the measured and calculated data, we compare possible matching conditions on $l_1$ and $l_2$ in Fig. 3. Each band shown in the figure defines the area of allowed $l_1$,$l_2$ pairs, which are consistent with one measurement/calculation of a magnetic moment. As $\mu_\mathrm{D}$ is insensitive to the $l_1$ term, it only constrained $l_2$. This constraint is shown by an horizontal band, with a width representing the total uncertainty, where we considered statistical and systematic errors in quadrature. At larger pion masses, an electromagnetically induced transition between the singlet and triplet bound states is allowed. The respective matrix element has been calculated with LQCD, and we can constrain the EFT with this additional input, $t_{01}$, via Eq. (11). The $\sim$4% uncertainty in $t_{01}$ translates with Eq. (11) into a relatively small uncertainty in $l_1$ compared with its calibration to $\mu_{^3\mathrm{H}}$ (compare red and blue band widths to the representative purple line width in Fig. 3). At physical $m_\pi$, this transition represents a breakup or fusion of a deuteron or a scattering neutron-proton singlet, respectively, but is not used here. The lattice predictions for $\mu_{^3\mathrm{H}}$ ($\mu_{^3\mathrm{He}}$) constrain the LECs to a negatively (positively) sloped band. The slope $dl_2/dl_1$ has the same magnitude but opposite sign, dependent upon whether $\mu_{^3\mathrm{H}}$ or $\mu_{^3\mathrm{He}}$ is used. This follows from the structure of the $l_1$ operator [Eq. (9)] whose isospin matrix element flips sign, while spin and coordinate-space matrix elements are identical at 806 MeV and almost equal at physical $m_\pi$.

Consistency between data and theory is attested in Fig. 3 by an overlap region of all four bands. The $l_2(l_1)$ dependencies shown in the figure are for extrapolations $\Lambda \to \infty$ from the interval 4–15 fm$^{-1}$ in which the necessary matrix elements were obtained. The EFT uncertainty is not explicit in the graph, but it is responsible for the three physical lines not intersecting in a point. In the $m_\pi = 806$ MeV case, we see a similar situation considering constraints due to magnetic moments. On the other hand, the transition matrix element $t_{01}$ seems to be inconsistent with the other observables, although still acceptable since it is within the current LQCD error bars.

### B. Three nucleons at $m_\pi = 450$ MeV

First, we discuss observables at $m_\pi = 450$ MeV, where we rely on interpolated values for $l_1$,$l_2$ because of insufficient data. For predictions in the three-nucleon sector one three-body observable is required to renormalize the EFT. No such datum has been calculated at $m_\pi = 450$ MeV. The magnetic moment of the triton, for example, can thus only be given as a function of its binding energy. This dependence is shown in Fig. 4 for the two unphysical pion masses at LO and NLO. First,

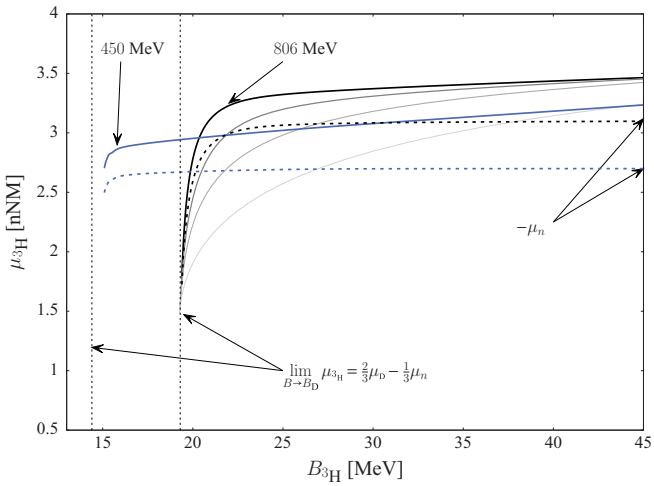


FIG. 4. The magnetic moment of the triton as a function of its binding energy for $m_\pi = 806$ MeV [gray ($\Lambda = 4$ fm$^{-1}$) $\rightarrow$ black ($\Lambda = 15$ fm$^{-1}$)] and $m_\pi = 450$ MeV (blue, $\Lambda = 8$ fm$^{-1}$). Vertical dashed lines mark the deuteron-neutron thresholds at $B_D = 19.5$ MeV and $B_D = 14.4$ MeV, respectively. LO results with one-body-current coupling (dotted lines) are compared with NLO values (solid lines) which consider also the two-body-current coupling $l_1$,$l_2$. Asymptotic limits are indicated with arrows, for $B_{^3\mathrm{H}} \rightarrow B_D$: $\mu_{^3\mathrm{H}} \rightarrow 1.196$ nNM (450 MeV), $\mu_{^3\mathrm{H}} \rightarrow 1.472$ nNM (806 MeV); and $B_{^3\mathrm{H}} \rightarrow \infty$: $\mu_{^3\mathrm{H}} \rightarrow 2.70$ nNM (450 MeV), $\mu_{^3\mathrm{H}} \rightarrow 3.119$ nNM (806 MeV).

we observe that with increasing $\Lambda$ (light gray to black solid line, NLO at $m_\pi = 806$ MeV; for $m_\pi = 450$ MeV and LO results the $\Lambda$ dependence is qualitatively the same and is not shown in Fig. 4) $\mu_{^3\mathrm{H}}$ rises discontinuously from the threshold energy $B_D$ to a constant at LO, while at NLO $\mu_{^3\mathrm{H}}$ rises linearly with $B_{^3\mathrm{H}}$. In the limit of $B_{^3\mathrm{H}} \rightarrow B_D$, i.e., for barely bound, very shallow states, all curves approach the naive limit $\mu_{^3\mathrm{H}} \sim 2/3\mu_D - 1/3\mu_n$ of a free deuteron-neutron system with appropriate spin orientation. For $B_{^3\mathrm{H}} \gg B_D$, LO results converge to the shell-model/Schmidt [32] values and thus provide a *deep* consistency check for the numerical method to produce the compact triton. The deviation $\delta\mu_{^3\mathrm{H}}$ from the Schmidt limit due to the photon coupling to the two-nucleon contact is about 15% and vanishes only at threshold. The critical binding energy at which $\delta\mu_{^3\mathrm{H}}$ changes linearly with $B_{^3\mathrm{H}}$ is about 2–4 MeV above threshold for the finite $\Lambda$s considered here. In the zero-range limit, this critical energy seems to converge to zero (consider the behavior at $m_\pi = 806$ MeV and NLO in Fig. 4) which indicates the aforementioned discontinuous transition from the free-particle to the shell-model approximate values of $\mu_{^3\mathrm{H}}$.

Assuming that $3/2B_D(450) < B_{^3\mathrm{H}}(450) < B_{^3\mathrm{H}}(806)$, the correlation in Fig. 4 yields the constraint

$$\mu_{^3\mathrm{H}} = 3 \pm 0.3 \text{ nNM} \quad \text{at } m_\pi = 450 \text{ MeV}. \tag{12}$$

A linear interpolation between $B_{^3\mathrm{H}}$'s at physical and 806 MeV $m_\pi$ suggests a central value of $B_{^3\mathrm{H}} = 29.7$ MeV.

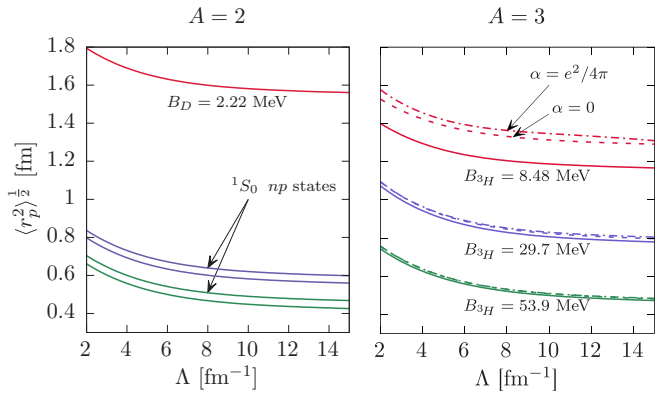


FIG. 5. Regulator dependence of the point-charge radii for the two- (left panel) and three-nucleon (right panel) bound states at the physical (red), 450 MeV (blue), and 806 MeV (green) pion masses. Solid lines refer to one-proton systems, i.e., the deuteron, $np$, and triton. Results for two-proton systems are shown with (dash-dotted) and without (dashed) electrostatic repulsion between the protons. For $A = 2$, the lines indicated with an arrow correspond to singlet $np$ state, while the lower solid lines mark the triplet deuteron.

### C. Charge radii

We shall employ the theory now to analyze the spatial distribution of nucleons within a nucleus at all three pion masses. Canonically, this is encoded in the radial moments of a nucleus. These moments are expansion coefficients of form factors. We consider the coupling of a nucleus to an external electric charge distribution which is parametrized with a charge form factor

$$F_C(q^2) = 1 - \frac{\langle r_p^2 \rangle}{6} q^2 + \cdots . \tag{13}$$

In leading order, it suffices to consider the one-body, scalar coupling via $\rho_{\text{ext}}$ [Eq. (1)], analogous to the leading contribution to the magnetic moment (see below). Two-body-current contributions to the charge radius appear at $O(Q^3)$ as described in Ref. [33], and thus the point-charge radius calculation for an $A$-nucleon bound state with $Z$ protons amounts to

$$\langle r_p^2 \rangle = \frac{1}{Z} \langle A | \sum_{i=1}^{A} \frac{1}{2}(1 + \tau_{z,i}) \mathbf{r}_i^2 | A \rangle. \tag{14}$$

We obtain the bound-state wave function as a solution of the Schrödinger equation in coordinate space with the above defined interaction. Nucleons are assumed to be pointlike in this approach, and hence the comparison with experiment becomes more favorable if the datum, the charge radius $\langle r_c^2 \rangle$, is corrected by a finite proton and neutron size:[2] $\langle r_c^2 \rangle = \langle r_p^2 \rangle + R_p^2 + N/(A - N)R_n^2$.

*The $A = 2$ case.* The dependence on the Gaussian regulator for all two-nucleon bound states at the physical and two unphysical pion masses is given in the left panel of Fig. 5. We find approximately the same $\Lambda$-convergence rate for the radii of the deuteron and the singlet $np$. In turn, the

[2] $R_p \approx 0.841$ fm and $R_n \approx -0.116$ fm, respectively.

difference between the respective values is $\Lambda$ independent, which reflects the variation in the binding energies, that are cutoff independent by construction.

The $np$ singlet states at larger pion masses are not as deeply bound as the triplet states. Binding-energy differences of $\delta B_{450} \sim 1.9$ MeV and $\delta B_{806} \sim 3.6$ MeV, respectively, result in charge radii which are different by an amount smaller than the EFT uncertainty.[3] With no electromagnetic repulsion between the protons, the charge radii of the proton-proton and neutron-proton singlets are identical. Even the effect of a Coulomb-induced splitting $B(np) - B(pp) = 0.5$ MeV (see discussion of $c_{pp}$ calibration) is found to be insignificant; i.e., $\langle r_c^2 \rangle$ of the now shallower di-proton is still almost identical to that of the $\alpha = 0$ scenario. Based on this observation, one would not expect LQCD predictions at 450 and 806 MeV $m_\pi$ of this observable to be affected strongly by dynamical QED.

*The $A = 3$ case.* The $\Lambda$ dependencies of the point-charge radii of the triton and $^3$He (Fig. 5) suggest again approximately equal theoretical EFT uncertainties for all pion masses, as inferred from the shape similarity of the respective curves. Again, the main motivation for this analysis is to assess the sensitivity of the observable with respect to electromagnetic interactions between the nucleons. At $m_\pi = 137$ MeV, the additional proton in $^3$He results in a significantly larger system, even if no Coulomb interaction is included. Note the difference to the two-nucleon case, where energetically degenerate $pp$ and $np$ singlets also have the same charge radius. For three nucleons, an identical binding energy for the triton and $^3$He, 8.48 MeV, does not produce the same charge radii. The effect of the Coulomb repulsion and the $c_{pp}$ counterterm, which is adjusted to the $pp$ scattering length, is relatively small, yet significant (dashed and dash-dotted lines). At $m_\pi = 450$ MeV, the respective differences in the radius between the triton and the charged and uncharged $^3$He are tiny. Finally, at $m_\pi = 806$ MeV, all three systems yield almost identical point-charge radii.

The results do not identify the binding energy as the main factor inducing the differences in this observable. This is apparent at physical $m_\pi$, where the uncharged $^3$He has the same binding energy as the triton. The latter is $\Lambda$ independent by construction, while the binding energy of the charged $^3$He nucleus is subject to a theoretical uncertainty within the considered $\Lambda$ range because it is the $pp$ scattering length ($m_\pi = 137$ MeV) or the $pp$ binding energies (unphysical $m_\pi$'s) which are used to renormalize $c_{pp}$. This residual $\Lambda$ dependence of $B_{^3\mathrm{He}}$ is not reflected in the results, as we find the shape of the corresponding dash-dotted curves in the right panel of Fig. 5 indistinguishable from those which represent systems with fixed binding energy.

In our analysis, we therefore identify the breaking of the Wigner SU(4) symmetry as the main source of this difference in the point-charge radii of $^3$H and $^3$He. For an SU(4) symmetric triton or helion we would expect the neutron point-charge radius to be identical to the proton point-charge radius, and to the matter radius. The breaking of this symmetry enlarges the radius of the majority species, since the $^1S_0$ channel is less attractive then the $^3S_1$ channel. At higher pion masses [18] the SU(4) symmetry is restored, and as a consequence we see the point proton charge radius difference shrinking with increasing pion mass.

The conclusion is the same as in the two-nucleon sector: the QED uncertainty in LQCD predictions of this observable at large pion masses is expected to be negligible.

*Comparing the $A = 2$ and 3 cases.* A comparison of radii in two- and three-nucleon systems supports the refutations of a correlation between system size, as measured by the point-charge radius, and binding energy. At $m_\pi = 137$ MeV, this correlation would still yield the correct hierarchy with the triton as the most deeply bound, and thus smallest, system, followed by $^3$He, which is not as deeply bound and larger, up to the largest and shallowest deuteron. In contrast, we find all three-nucleon systems larger in size at the unphysical pion masses relative to the $np$ bound states, despite the fact that the latter are more weakly bound. At $m_\pi = 450$ MeV, two- and three-nucleon systems have approximately the same charge radius. The counterintuitive ordering of two- and three-nucleon radii is a first indication of the peculiarity of the $NN$ system at $m_\pi = 806$ MeV. Below, we will comment on the polarizability as another instance of an unexpected response of the $NN$ system. To conclude this section, we note that the orderings are unaffected by the regularized Coulomb interaction and consequently should be characteristics of the strong interaction.

### D. Magnetic moments

In Table III we present the evolution of the nuclear magnetic moments in EFT($\not\pi$). The values of the shell-model approximation yield the magnetic moment as the sum of the single-particle contributions with appropriate spin orientations. This simple approximation works well, within 15% for $m_\pi = 137$ MeV and $m_\pi = 806$ MeV, for all considered nuclei. We then consider the coupling of the LO EFT($\not\pi$) magnetic one-body currents to a bound nucleus, as a first refinement of the shell model. As expected, the deuteron magnetic moment is unaffected. However, the agreement between theory and data gets worse for the $A = 3$ nuclei, particularly at the physical pion mass. To understand this result, we should return to the discussion in Sec. III B and consider the competing pictures of a compact $A = 3$ nucleus versus a shallow cluster state composed of a neutron or proton orbiting around a deuteron. For a compact nucleus, the single-particle picture, $\mu_{^3\mathrm{H}} = \mu_p$ and $\mu_{^3\mathrm{He}} = \mu_n$, dominates. For a clustered state, we expect that $\mu_{^3\mathrm{H}} \longrightarrow (2/3\mu_\mathrm{D} - 1/3\mu_n)$ as $B_{^3\mathrm{H}} \to B_\mathrm{D}$, and therefore we expect to obtain a smaller magnetic moment (this argument applies equally to $^3$He). This explanation is consistent with the difference in binding energies between the rather shallow trimers at the physical pion mass, and the deeply bound $m_\pi = 806$ MeV trimers.

The two-body magnetization current that appears at NLO reconciles the theory with the available data. For the physical case we see an agreement at the 2 permille level. This might not be that impressive, as $l_1$ was fitted to reproduce the $^3$H magnetic moment. In contrast the $A = 3$ results for the $m_\pi = 806$ MeV

[3] A lower bound of which is given by the difference of the radii obtained at smallest and largest $\Lambda$, i.e., about 0.3 fm (see Table II).

TABLE III. The evolution of the magnetic moments (in nNM) of the $A = 2,3$ nuclei in EFT($\not\pi$) for $m_\pi = 137$ MeV and $m_\pi = 806$ MeV. The LECs at $m_\pi = 137$ (806) MeV where calibrated using $\mu_D$ and $\mu_{^3H}$ ($\mu_D$ and $t_{01}$).

| | $m_\pi = 137$ MeV | | | $m_\pi = 806$ MeV | | |
|---|---|---|---|---|---|---|
| | deuteron | triton | helion | deuteron | triton | helion |
| Shell model | 0.879 | 2.793 | −1.913 | 1.138 | 3.119 | −1.981 |
| LO | 0.879 | 2.746 | −1.862 | 1.138 | 3.118 | −1.979 |
| NLO | 0.857 | 2.979 | −2.130 | 1.220 | 3.405 | −2.170 |
| Expt./LQCD | 0.857 | 2.979 | −2.127 | 1.220(95) | 3.56(19) | −2.29(12) |

case are predictions of our theory, and it can be seen that they agree with the LQCD data within error bars.

The discrepancy between the nuclear magnetic moments and theoretical predictions relaying on the one-body magnetization current, only, have a history in nuclear physics. It was suggested, for example, that a $d$-wave admixture in the nuclear wave function can resolve this discrepancy; see, e.g., Ref. [4]. The wave function in LO EFT($\not\pi$) of the $A = 2,3$ nuclei, however, has no $d$-wave component. Therefore, such explanations are excluded from our theory. As we have shown, this limitation is compensated by the two-body currents, that reconcile the theory with the experimental/LQCD data.

### E. Magnetic polarizabilities

In general, polarizabilities parametrize the second-order response of a system to an external probe. The dominant terms, which are quadratic in the magnetic field, are provided in the EFT($\not\pi$) formalism by an additional insertion of the one- and two-body magnetic-moment couplings as given in Eq. (8) and (9). The system is thereby subjected to the probe at different points in spacetime, and the polarizability is then sensitive to its deformation. In coordinate-space Schrödinger-equation practice, the calculation is analogous to a second-order perturbation of the energy; see Appendix C. Again, the zero-range approximation in the two-nucleon case allows for an analytic derivation of the cutoff dependence of this quantity. This estimate was made in [34], and yields a cutoff-independent polarizability of the deuteron.

The results for the magnetic polarizability of the deuteron $\beta_D$, triton $\beta_{^3H}$, and helium $\beta_{^3He}$ are listed in Table II. In Figs. 6 and 7, we compare the regulator dependence of the polarization for the two $A = 3$ mirror nuclei: $^3$He and triton at $m_\pi = 137$ MeV and $m_\pi = 806$ MeV. The functional dependence for interpolating the data points was chosen as $a_1 + a_2/\Lambda^2$, where $a_1$ and $a_2$ are two constants employed to fit the data. The numerical accuracy, indicated by error bars in the figures, was used as a measure of the importance of the different data points in the fit.

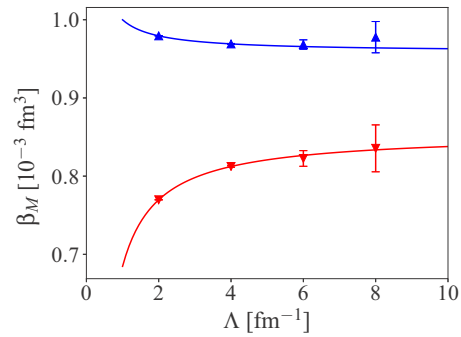


FIG. 6. Regulator dependence of the magnetic polarizability EFT calculations for $^3$He and triton $m_\pi = 137$ MeV.

At $m_\pi = 137$ MeV, our postdictions for $\beta_D$ are consistent with previous theoretical analyses and extractions based on cross-section data (see Table II). The absolute value of $\beta_D$ is two orders of magnitude larger than the single-nucleon polarizabilities and justifies, in part, why we call the deuteron a shallow nucleus. Our predictions[4] for $\beta_{^3H}$ and $\beta_{^3He}$ signify relatively compact, rigid three-nucleon bound states because they are of the same order of magnitude as $\beta_{n/p}$.

At $m_\pi = 806$ MeV, all polarizabilities—neutron/proton, deuteron (with $j_z = \pm 1$), and the three-nucleon states—are found by LQCD to be of the same order of magnitude. In particular, this entails a deuteron, which is by that measure as rigid and compact as the one- and three-nucleon states. This rigidity is consistent with the relatively large deuteron binding energy at $m_\pi = 806$ MeV. The EFT postdictions, in turn, suggest a different response. For $j_z = \pm 1$ we get $\beta_D \approx 0$, but for $j_z = 0$ we find $\beta_D$ to be two orders of magnitude larger than $\beta_{p/n}$ and therefore relatively pliant, as at $m_\pi = 137$ MeV. Furthermore, we postdict $\beta_{^3H}$ and $\beta_{^3He}$ to be an order of magnitude smaller than the LQCD predictions. Even the relatively large numerical uncertainty (see $\beta_{^3H}$ at $\Lambda = 8$ fm$^{-1}$ in Fig. 7) cannot account for this difference.

If we interpret the lattice results such that the polarizabilities of composite nuclei are dominated by the rigidity of the constituents and almost independent of binding effects, the discrepancy seems logical because the EFT considers nucleons as pointlike objects. Hence, the EFT description ignores their shape distortion in the external field and reflects only the effect on the relative positions of the constituents. The heuristic picture, suggested by the lattice calculations, of nuclei composed of very pliant nucleons refutes the intuitive caricature of a dense package of rigid spheres, and represents a challenge for the EFT description.

[4]To our knowledge, these numbers are first-time predictions and thus cannot be compared with others.

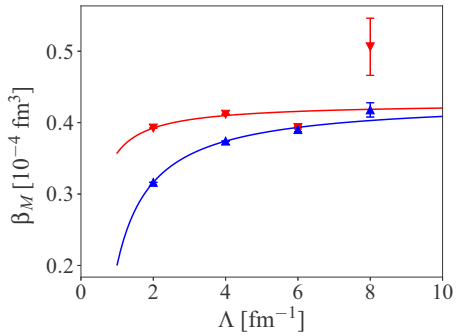


FIG. 7. Regulator dependence of the magnetic polarizability EFT calculations for $^3$He and triton $m_\pi = 806$ MeV.

## IV. SUMMARY

We have analyzed the pion-mass dependence of magnetic moments, charge radii, and polarizabilities of the deuteron, triton, and helion as characteristics of nuclei in external electromagnetic fields. The observables were calculated model independently according to the pionless-effective-field-theory formalism as developed for physical few-nucleon systems. For unphysical pion masses, calculations were based on a previously applied match of this theory to lattice QCD data. The robustness of the results with respect to different models to account for the electromagnetic interaction within two-proton systems was assessed.

Results which pertain to physical nuclei are consistent with data and previous calculations. The polarizabilities of the triton and helion are included as predictions awaiting experimental verification.

For the analysis of lattice data at $m_\pi = 450$ MeV, we calculated the dependence of the triton's magnetic moment on its binding energy. This dependence is found to approach the shell-model limit at large binding energies and to decrease linearly up to a discontinuity at the deuteron-neutron threshold. The relatively small slope of the linear dependence leads to a prediction of the magnetic moment of the triton and helion. A conjectured triton binding energy based on this prediction is found consistent with a linear dependence of this energy on the pion mass.

Charge radii and magnetic moments of two-proton nuclei are found to be insensitive with respect to different models for the electromagnetic interaction between constituent protons relative to the accuracy which is expected from a NLO EFT analysis. Nuclei at larger pion masses are found to be more robust in the two scenarios we used to estimate the effect of dynamical QED.

In terms of the magnetic polarizability, we found the deuteron to be much more pliable relative to the one- and three-nucleon QCD calculations, and of the same order of magnitude as the physical deuteron.

## ACKNOWLEDGMENTS

We are very grateful for illuminating discussions with B. C. Tiburzi. This work was supported by the Israel Science Foundation (Grant No. 1308/16), the Pazi Research Foundation, and the NSF (Grant No. PHY15-15738).

## APPENDIX A: THE LOW ENERGY CONSTANTS

In Table IV we list the LECs used in our calculations.

TABLE IV. The LECs $c_{S,T,pp}^{\Lambda}$, $d_3^{\Lambda}$ (GeV) and $l_{1,2}^{\Lambda}$ (n.d.) for physical ($m_\pi = 140$ MeV) and lattice ($m_\pi = 450,\ 806$ MeV) nuclei for various values of the momentum cutoff $\Lambda$ (fm$^{-1}$).

| $m_\pi$ | $\Lambda$ | $c_T^{\Lambda}$ | $c_S^{\Lambda}$ | $d_3^{\Lambda}$ | $c_{pp}^{\Lambda}$ | $l_1$ | $l_2$ |
|---|---|---|---|---|---|---|---|
| 140 | 2 | − 0.1423 | − 0.1063 | 0.06849 | − 0.0008303 | 2.530 | − 0.4652 |
| | 4 | − 0.5051 | − 0.4350 | 0.6778 | − 0.007646 | 0.7349 | − 0.1086 |
| | 6 | − 1.091 | − 0.9863 | 2.653 | − 0.01685 | 0.3588 | − 0.04717 |
| | 8 | − 1.899 | − 1.760 | 7.816 | − 0.02750 | 0.2125 | − 0.02617 |
| | 10 | − 2.929 | − 2.757 | 20.48 | − 0.03917 | 0.1403 | − 0.01660 |
| | 12 | − 4.182 | − 3.976 | 50.94 | − 0.05202 | 0.09932 | − 0.01152 |
| | 15 | − 6.480 | − 6.222 | 195.6 | − 0.07200 | 0.06470 | − 0.007324 |
| 450 | 2 | − 0.1637 | − 0.1574 | 0.1580 | − 0.003267 | 2.023 | 0.0288 |
| | 4 | − 0.4837 | − 0.4730 | 0.8374 | − 0.009155 | 0.556 | − 0.00168 |
| | 6 | − 0.9741 | − 0.9591 | 2.711 | − 0.01653 | 0.269 | − 0.00207 |
| | 8 | − 1.635 | − 1.616 | 7.182 | − 0.02494 | 0.160 | − 0.00150 |
| | 10 | − 2.466 | − 2.443 | 17.33 | − 0.03422 | 0.106 | − 0.00107 |
| | 12 | − 3.468 | − 3.440 | 40.04 | − 0.04421 | 0.075 | − 0.000843 |
| | 15 | − 5.291 | − 5.256 | 137.0 | − 0.06032 | 0.049 | − 0.000579 |
| 806 | 2 | − 0.1480 | − 0.1382 | 0.07102 | − 0.002125 | 1.476 | 0.5907 |
| | 4 | − 0.4046 | − 0.3885 | 0.3539 | − 0.006886 | 0.3017 | 0.1199 |
| | 6 | − 0.7892 | − 0.7668 | 1.001 | − 0.01298 | 0.1242 | 0.0492 |
| | 8 | − 1.302 | − 1.273 | 2.221 | − 0.02007 | 0.06710 | 0.02656 |
| | 10 | − 1.942 | − 1.907 | 4.308 | − 0.02814 | 0.04194 | 0.01660 |
| | 12 | − 2.710 | − 2.670 | 7.712 | − 0.03676 | 0.02860 | 0.01130 |
| | 15 | − 4.103 | − 4.052 | 16.84 | − 0.05077 | 0.01805 | 0.007092 |

## APPENDIX B: MAGNETIC MOMENTS IN THE ZERO-RANGE LIMIT

The analysis of the two-nucleon system based on an interaction constrained by a single datum, namely the deuteron binding energy, was instigated almost a century ago in Ref. [35]. What later became known as the zero-range approximation can be used here to derive analytically the dependence of the two-body-current LECs $l_1$,$l_2$ as introduced in Eqs. (1) and (9).

The bound-state solution of the Schrödinger equation in an area of vanishing potential reads

$$\langle r|\mathrm{BS}\rangle = \frac{A_S}{\sqrt{4\pi}}\frac{e^{-\kappa r}}{r}, \tag{B1}$$

where $A_s$ is the wave function normalization and $\kappa = \sqrt{mB}$ is set by the deuteron's (dineuteron's) binding energy $B_D$ ($B_{nn}$).

The contribution of the one-body current as parametrized in Eq. (8) is evaluated to be

$$\langle \mathrm{BS}|\boldsymbol{\mu}^{(1)}|\mathrm{BS}\rangle = \frac{A_S^2}{2\kappa}\mu_N(g_p+g_n). \tag{B2}$$

Similarly, the two-body current regularized with a Gaussian, Eq. (9), yields the following result for the spin-triplet state:

$$\langle \mathrm{BS}|\boldsymbol{\mu}^{(2)}|\mathrm{BS}\rangle = {A_s}^2\mu_N l_2\Lambda^2. \tag{B3}$$

Cutoff independence implies $l_2 \propto \Lambda^{-2}$. This regulator dependence was found above (see discussion of Fig. 1) numerically. We can coepmpare these expressions with the EFT($\not\pi$) calculation of [6] where the authors used a power-divergence-subtraction method introducing a dimensional regularization scale $\mu$,

$$\mu_D = \mu_N(g_p+g_n) + \tilde{l}_2\sqrt{mB_D}(\mu-\sqrt{mB_D})^2. \tag{B4}$$

These results coincide in the zero-range limit where in which the asymptotic wave function is normalized to 1, and $A_S^2 \to 2\sqrt{mB_D}$. The $\mu$ dependence of the NLO LEC can be determined for arbitrary values of $\mu$ but will coincide with the $\Lambda$ dependence for $\mu \gtrsim m_\pi$.

## APPENDIX C: MAGNETIC POLARIZABILITIES

The calculation of polarizabilities as parametrizations of the second-order response of a nucleus (spin-quantum numbers $j_0$,$m_0$) to perturbation given by its coupling to an external magnetic field is explained here. Specifically, the twice-iterated coupling of the photon to the nucleus shifts its energy by an excitation of intermediate states $n$:

$$\begin{aligned}\Delta E^{(2)} &= \sum\!\!\!\!\!\!\int_n \frac{\langle j_0 m_0|\boldsymbol{\mu}\cdot\boldsymbol{B}|j_n m_n\rangle\langle j_n m_n|\boldsymbol{\mu}\cdot\boldsymbol{B}|j_0 m_0\rangle}{E_n - E_0} \\ &\equiv \frac{1}{2}\sum_{\lambda\nu}(-)^\nu \beta_\nu^{(\lambda)} B_\nu^{(\lambda)}.\end{aligned} \tag{C1}$$

Thereby, the spherical components of the polarizability

$$\begin{aligned}\beta_\nu^{(\lambda)} &= \frac{2}{3}\sum\!\!\!\!\!\!\int_n \frac{|\langle j_0||\boldsymbol{\mu}||j_n\rangle|^2}{E_n - E_0} \\ &\times \sum_q (-)^q \langle j_0 m_0 j_n m_n|1q\rangle^2 \langle 1q\,1-q|\lambda\nu\rangle,\end{aligned} \tag{C2}$$

and the quadratic field tensor

$$B_\nu^{(\lambda)} = (-)^\nu \sum_{pq}\langle 1p1q|\lambda\nu\rangle B_p B_q \tag{C3}$$

are defined. For $\boldsymbol{B} = B\boldsymbol{e}_z$, the expression of the shift in terms of scalar and tensor polarizability is

$$\Delta E^{(2)} = \left(-\frac{1}{2\sqrt{3}}\beta_0^{(0)} + \frac{1}{\sqrt{6}}\beta_0^{(2)}\right)B^2 \tag{C4}$$

with

$$\begin{aligned}\beta_0^{(0)} &= -\frac{2}{3}\frac{\sqrt{3}}{2j_0+1}\sum\!\!\!\!\!\!\int_n \frac{|\langle j_0||\boldsymbol{\mu}||j_n\rangle|^2}{E_n - E_0}, \\ \beta_0^{(2)} &= -12\sqrt{5}\frac{m_0^2 - \frac{1}{3}j_0(j_0+1)}{\sqrt{(2j_0+3)(2j_0+2)\cdots(2j_0-1)}} \\ &\times \sum\!\!\!\!\!\!\int_n \frac{|\langle j_0||\boldsymbol{\mu}||j_n\rangle|^2}{E_n - E_0}\mathsf{W}(j_n j_0 12; 1 j_0).\end{aligned} \tag{C5}$$

Weighted with Racah's $\mathsf{W}$ coefficient, we combine matrix elements for the allowed transition, where care has to be taken to include the additional $j_n = 0$ bound states at the unphysical $m_\pi$. The definition of scalar and tensor polarizabilities is then identical to that used in Ref. [19].


[1] J. M. B. Kellogg, I. I. Rabi, N. F. Ramsey, and J. R. Zacharias, The magnetic moments of the proton and the deuteron. The radiofrequency spectrum of $H_2$ in various magnetic fields, Phys. Rev. **56**, 728 (1939).

[2] A. Landé, Nuclear magnetic moments and their origin, Phys. Rev. **46**, 477 (1934).

[3] R. G. Sachs, The magnetic moments of light nuclei, Phys. Rev. **69**, 611 (1946).

[4] R. G. Sachs and J. Schwinger, The magnetic moments of $H^3$ and $He^3$, Phys. Rev. **70**, 41 (1946).

[5] U. van Kolck, Effective field theory of short range forces, Nucl. Phys. A **645**, 273 (1999).

[6] J.-W. Chen, G. Rupak, and M. J. Savage, Nucleon-nucleon effective field theory without pions, Nucl. Phys. A **653**, 386 (1999).

[7] D. B. Kaplan, M. J. Savage, and M. B. Wise, Two-nucleon systems from effective field theory, Nucl. Phys. B **534**, 329 (1998).

[8] D. B. Kaplan, M. J. Savage, and M. B. Wise, A new expansion for nucleon-nucleon interactions, Phys. Lett. B **424**, 390 (1998).

[9] P. F. Bedaque, H. W. Hammer, and U. van Kolck, Effective theory of the triton, Nucl. Phys. A **676**, 357 (2000).
[10] W. E. Caswell and G. P. Lepage, Effective Lagrangians for bound state problems in QED, QCD, and other field theories, Phys. Lett. B **167**, 437 (1986).
[11] X. Kong and F. Ravndal, Proton proton fusion in leading order of effective field theory, Nucl. Phys. A **656**, 421 (1999).
[12] J. Kirscher and D. Gazit, The Coulomb interaction in helium-3: Interplay of strong short-range and weak long-range potentials, Phys. Lett. B **755**, 253 (2016).
[13] S. König, H. W. Grießhammer, H. W. Hammer, and U. van Kolck, Effective theory of $^3$H and $^3$He, J. Phys. G **43**, 055106 (2016).
[14] B. Bazak, M. Eliyahu, and U. van Kolck, Effective field theory for few-boson systems, Phys. Rev. A **94**, 052502 (2016).
[15] N. Barnea, W. Leidemann, and G. Orlandini, State dependent effective interaction for the hyperspherical formalism, Phys. Rev. C **61**, 054001 (2000).
[16] N. Barnea, W. Leidemann, and G. Orlandini, State-dependent effective interaction for the hyperspherical formalism with noncentral forces, Nucl. Phys. A **693**, 565 (2001).
[17] H. Hofmann, in *Proceedings of Models and Methods in Few-Body Physics, Lisboa, Portugal*, edited by L. Ferreira, A. Fonseca, and L. Streit (Springer, Berlin, 1986), p. 243.
[18] J. Kirscher, N. Barnea, D. Gazit, F. Pederiva, and U. van Kolck, Spectra and scattering of light lattice nuclei from effective field theory, Phys. Rev. C **92**, 054002 (2015).
[19] E. Chang, W. Detmold, K. Orginos, A. Parreno, M. J. Savage, B. C. Tiburzi, and S. R. Beane, Magnetic structure of light nuclei from lattice QCD, Phys. Rev. D **92**, 114502 (2015).
[20] P. J. Mohr, B. N. Taylor, and D. B. Newell, Codata recommended values of the fundamental physical constants: 2010, Rev. Mod. Phys. **84**, 1527 (2012).
[21] S. R. Beane, E. Chang, W. Detmold, K. Orginos, A. Parreno, M. J. Savage, and B. C. Tiburzi, Ab Initio Calculation of the $np \to d\gamma$ Radiative Capture Process, Phys. Rev. Lett. **115**, 132001 (2015).
[22] K. Orginos, A. Parreno, M. J. Savage, S. R. Beane, E. Chang, and W. Detmold (NPLQCD Collaboration), Two-nucleon systems at $m_\pi \sim 450$ MeV from lattice QCD, Phys. Rev. D **92**, 114512 (2015).
[23] A. Parreno, M. J. Savage, B. C. Tiburzi, J. Wilhelm, E. Chang, W. Detmold, and K. Orginos, Octet baryon magnetic moments from lattice QCD: Approaching experiment from the three-flavor symmetric point, Phys. Rev. D **95**, 114513 (2017).
[24] S. R. Beane, E. Chang, S. D. Cohen, W. Detmold, H. W. Lin, T. C. Luu, K. Orginos, A. Parreno, M. J. Savage, and A. Walker-Loud, Light nuclei and hypernuclei from quantum chromodynamics in the limit of SU(3) flavor symmetry, Phys. Rev. D **87**, 034506 (2013).
[25] M. Gorchtein, New Sum Rule for the Nuclear Magnetic Polarizability, Phys. Rev. Lett. **115**, 222503 (2015).
[26] J. L. Friar and G. L. Payne, Higher-order nuclear-polarizability corrections in atomic hydrogen, Phys. Rev. C **56**, 619 (1997).
[27] J.-W. Chen, H. W. Grießhammer, M. J. Savage, and R. P. Springer, The polarizability of the deuteron, Nucl. Phys. A **644**, 221 (1998).
[28] I. Angeli and K. P. Marinova, Table of experimental nuclear ground state charge radii: An update, At. Data Nucl. Data Tables **99**, 69 (2013).
[29] J. Vanasse, The triton charge radius to next-to-next-to-leading order in pionless effective field theory, Phys. Rev. C **95**, 024002 (2017).
[30] J. Kirscher, H. W. Grießhammer, D. Shukla, and H. M. Hofmann, Universal correlations in pion-less EFT with the resonating group model: Three and four nucleons, Eur. Phys. J. A **44**, 239 (2010).
[31] J. Vanasse, D. A. Egolf, J. Kerin, S. König, and R. P. Springer, $^3$He and $pd$ scattering to next-to-leading order in pionless effective field theory, Phys. Rev. C **89**, 064003 (2014).
[32] T. Schmidt, Über die Magnetischen Momente der Atomkerne, Z. Phys. **106**, 358 (1937).
[33] M. P. Valderrama and D. R. Phillips, Power Counting of Contact-Range Currents in Effective Field Theory, Phys. Rev. Lett. **114**, 082502 (2015).
[34] J. Drachman, Magnetic Properties of Nuclear Two-Body Systems in the Zero-Range Approximation for LQCD, MSc thesis, The Racah Institute of Physics, The Hebrew University of Jerusalem, 2016.
[35] H. Bethe and R. Peierls, Quantum theory of the diplon, Proc. R. Soc. London A **148**, 146 (1935).